Inter*net* Electronic Journal*

Nanociencia et Moletrónica

Diciembre 2012, Vol.10, N°2, pp 1927-1944

Strong and weak quantum confinement of nanocrystalline PbS thin films doping Ni^{2+} and Cd^{2+} by Chemical Bath

[1]G. Hernández Téllez, [1]R. Gutiérrez Pérez, [2]M. Hernández Hernández, [2]J. Hernández Tecorralco, [3]A. Carbajal Ortiz, [2]M. Zamora Tototzintle, [2]S. Zamora Zamora, [2]L. Chatel Lima, [2*]O. Portillo Moreno.

1. Lab. Síntesis de Complejos, Facultad de Ciencias Químicas, Benemérita Universidad Autónoma de Puebla. P.O. Box 1067, Puebla, Pué., 72001 México. 2. Lab. de Ciencias de Materiales de la Facultad de Ciencias Químicas BUAP C. U. Tel. (01 222) 2 29 55 00 Ext. 7519. Puebla, México.
3. Departamento de Ciencias Básicas del Instituto Tecnológico de Ciudad Juárez Chihuahua, México, Av. Tecnológico 1340 Col. el Crucero, C. P. 32500, tel. 01656 6882500.

recibido: 6.6.2012 revisado: 22.06.12 publicado: 31.12.12

Citation of the article;
G. Hernández Téllez, R. Gutiérrez Pérez, M. Hernández Hernández, J. Hernández Tecorralco, [3]A. Carbajal Ortiz, M. Zamora Tototzintle, S. Zamora Zamora, L. Chatel Lima, O. Portillo Moreno. Strong and weak quantum confinement of nanocrystalline PbS thin films doping Ni^{2+} and Cd^{2+} by Chemical Bath,Int. Electron J. Nanoc. Moletrón, 2012, Vol. 10, N°2, pp 1927-1944

Strong and weak quantum confinement of nanocrystalline PbS thin films doping Ni^{2+} and Cd^{2+} by Chemical Bath

[1]G. Hernández Téllez, [1]R. Gutiérrez Pérez, [2]M. Hernández Hernández, [2]J. Hernández Tecorralco, [3]A. Carbajal Ortiz, [2]M. Zamora Tototzintle, [2]S. Zamora Zamora, [2]L. Chatel

1. Lab. Síntesis de Complejos, Facultad de Ciencias Químicas, Benemérita Universidad Autónoma de Puebla. P.O. Box 1067, Puebla, Pué., 72001 México.2. Lab. de Ciencias de Materiales de la Facultad de Ciencias Químicas BUAP C. U. Tel. (01 222) 2 29 55 00 Ext. 7519. Puebla, México.
3. Departamento de Ciencias Básicas del Instituto Tecnológico de Ciudad Juárez Chihuahua, México, Av. Tecnológico 1340 Col. el Crucero, C. P. 32500, tel. 01656 6882500.

recibido: 6.6.2012 revisado: 22.06.12 publicado: 31.12.12

Internet Electron. J. Nanoc. Moletrón., 2012, Vol.10 , N° 2, pp 1927-1944

Abstract: The growth of nanocrystalline PbS films doped Cd^{2+} and Ni^{2+} by chemical bath deposition (CBD) onto glass at temperature T = 20± 2°C, is presented in this research. We report on the modification of structural and optical nanostructures due to in situ Ni^{2+} and Cd^{2+} doping. The morphological changes of the layers were analyzed by Scanning Electron Microscopy (SEM). XRD spectra displayed peaks at 2θ = (26.00, 30.07, 43.10, 51.00, 53.48), indicating growth on the zinc blende face. The grain size determined by x-rays diffraction of the Cd^{2+} samples was found ~36-30 nm, whereas with the doped Ni^{2+} sample 36-5 nm.Optical absorption spectra, forbidden band gap energy (E_g) for Ni^{2+} shift disclose a shift in the range 2.1-3.8 eV. A shift of excitonic peak towards higher energy with an increased in Cd^{2+} concentration is also observed. Optical Absorption Spectra show for Cd^{2+} and Ni^{2+} a redshift of the forbidden band gap of 0.34-0.51 eV and band gap of films doped varied from 2.1-4.0 eV. We observe a strong quantum confinement PbSNi films and weak quantum confinement PbSCd films
Keywords: Thin films, doping, potential cell, Gibbs free energy, coordination complex.

Resumen: El crecimiento de películas PbS nanocristalinas dopadas con Cd^{2+} y Ni^{2+} mediante la técnica de deposito por baño químico (DBQ), sobre sustratos de vidrio a temperatura de 20± 2°C es presentada en esta investigación. Presentamos la modificación óptica y nanostructural del dopamiento con Cd^{2+} y Ni^{2+} in-sintu. Los cambios morfológicos de las capas fueron analizados por Microscopia Electrónica de Barrido (MEB). Los espectros de Difracción de Rayos X (DRX) muestran picos en las posiciones angulares: 2θ = (26.00, 30.07, 43.10, 51.00, 53.48). El tamaño de grano fue determinado por DRX para las dopadas con Cd^{2+} se encontró en ~36-30 nm, mientras que para las dopadas con NI^{2+} ~36-5 nm. Los espectros de absorción óptica, el ancho de energía de banda prohibida (E_g) para Ni^{2+} muestra un corrimiento en el intervalo de 2.1-3.8 eV. El corrimiento del pico excitonico hacia alta energía con el incremento de la concentración del dopante Cd^{2+} y Ni^{2+} es observada. Los espectros de de absorción óptica muestran para Cd^{2+} y Ni^{2+} corrimiento en E_g varia de 0.34-0.51 eV y 2.1-4.0 eV. Nosotros observamos efecto de confinamiento cuántico fuerte en películas PbSNi y efecto de confinamiento cuántico débil en películas PbSNi.

Palabras clave: Películas delgadas, dopante, potencial de celda, Energía libre de Gibbs, complejo de coordinación.

1. Introduction

The ever-increasing interest into deposition of ternary derivative materials, the potential of designing and tailoring both the lattice parameters and the forbidden band-gap energy (E_g) by controlling growth parameters [1, 2]. In this regard, many techniques have been successfully employed: successive ionic layer and reaction (SILAR) [3, 4] etc. Most of the studies reported so far have focused in the deposition of ternary derivatives material in thin films as $Cd_{1-x}Zn_xS$ [5], $Cd_{1-x}SCu_x$ [6], $Hg_xCd_{1-x}S$ [7]. Noteworthy is the fact that PbS thin films are promising photovoltaic materials as their variable E_g can be adjusted to match the ideal ~1.5 eV required for achieving a most efficient solar cell [8], likewise size-dependent new physical aspects have generated an ongoing thrust for new practical applications and PbS nanocrystals with grain-size (GS) dimensions in the range 1-20 nm are of technological interest for advanced optoelectronic applications, showing a stronger quantum confinement effect when the crystallite size matches the dimension of Bohr exciton [9]. In this context, there are two situations, called the weak confinement and the strong regimes [10]. In the weak regime the particle radius of the electron-hole pair, but the range of motion of the exciton is limited, which causes a blue shift in the absorption spectrum. When the size of the nanoparticles are below Bohr radius, its lead to the quantum confinement effect. This confinement induces discrete electronic states in the valence and conduction band of the quantum dots compared to the continuous state of energy in bulk material. If the crystallite size is below the exciton Bohr of the semiconductor, strong quantum confinement occurs. The confinement effect appears as a shift in absorption spectra and the absorption to lower wavelengths, wicks is due to change in the E_g [11, 12] and control over assembly through modification of surface functionalization. On the other hand, photovoltaic's devices are an widely recognized potential application for nanocrystals due, in part, to their high photoconductivity, easy work-up for solutions and also low cost of production. Several schemes for using nanocrystals in solar cells are under active consideration, including nanocrystals-polymer composites [13, 14]. In this regard, growing interest has been devoted to the Pb-chalcogenide family for nanocrystals solar cell applications because they have such large exciton Bohr radii of 18 nm, in the limit where the nanocrystals are only a tenth part or so of the bulk exciton diameter: electrons and holes can then tunnel through a thin surface coating, and therefore strong electronic coupling between particles allows the transport of charge between nanocrystals. The quantized electronic transitions in Pb(S, Se) nanocrystals quantum dots (NQDs) have been reported to provide size-tunable interband absorption and luminescence emission at a broad and technically important infrared wavelength range, spanning from 0.8-4.0μm [15]. It must be pointed out that the synthesis of ternary $Pb_{1-x}Ni_xS$ and $Pb_{1-x}Cd_xS$ nanocrystals remains largely underdeveloped compared to the widely studied cadmium chalcogenide. Thus, on this frame of reference, in the present work attempt has been made to prepare PbS Ni^{2+} and Cd^{2+} doped PbS nanostructured films by chemical bath deposition (CBD), in order to investigate structural and optical of undoped and doped-PbS films. Surface morphology and composition were determined using a Carl Zeiss Auriga 39-16 coupled with a Bruker energy dispersive analysis of X-Rays (EDAX). The crystalline structure characterization was carried out by XRD patterns registered in a D8 Discover diffractometer, using the Cu K_α line. The grain size was determined utilizing the Scherer's formula on XRD patterns. The optical absorption spectra, measured employing a Unicam 8700 Spectrometer, allow to calculate the forbidden band gap energy (E_g) by using

the $(\alpha h\nu)^2$ vs. $h\nu$ plot, where α is the optical absorption coefficient and $h\nu$ the photon energy.

2. Chemical reactions and experimental procedure

The reactions for the growth of PbS films doped with Ni^{2+} and Cd^{2+} were determined by employing the cell potential values in basic media reported [16] A. The cell potential and the Gibbs free energy are related through the Nernst equations: $\Delta G^o = -n\tau\varepsilon^o$, where *n* is the number of equivalents, τ is the Faraday constants and ε^o are the cell potential, ΔG^o is calculated for the reaction. Value ΔG^o provides thermodynamic information on the spontaneity of chemical reactions. Worth-noting is the formation of the coordination complex $[M(NH_3)_4]^{2+}$, which is determinant for the release of M^{2+} ions (M^{2+} = Cd^{2+}, Pb^{2+}, Zn^{2+}, etc.) and their slow recombination with S^{2-} ions that, under these conditions, leads to the spontaneous formations to the MS precipitate in an easily controlled process. The growth of PbS is therefore carried out according to the following steps: (*a*) by mixing $Pb(CH_3CO_3)_2$, KOH and NH_4NO_3, the coordination complex $[Pb(NH_3)_4]^2$ is generated indirectly. (*b*) The S^{2-} ions are found in the solution and are generated by the thiourea decomposition in alkaline solution. (*c*) The aforementioned steps allow the slow process at the substrate surface to take place predominantly over direct hydrolysis of thiourea in the bulk of the reaction bath as follow [17]

$$SC(NH_2)_2 + 3OH^- \Leftrightarrow CH_2N_2 + CO_3^{2-} + H_2S + 3H^+ \quad (1)$$

$$HPbO_2^- + H_2O + 2e \Leftrightarrow Pb + 3OH^- \qquad \Delta G^0 = +104.2\text{KJ} \quad (2)$$

Leading to complex (II)

$$[Pb(NH_3)_4]^{2+} + 2e \Leftrightarrow Pb + 4NH_3 \qquad \Delta G^o = +180.3\text{ KJ} \quad (3)$$

$$Pb^{2+} + 2e \Leftrightarrow Pb \qquad \Delta G^o = +24.31\text{KJ} \quad (4)$$

Changing the sense of (4) and added with (3)

$$[Pb(NH_3)_4]^{2+} \Leftrightarrow Pb^{2+} + 4NH_3 \qquad \Delta G^o = +155.99\text{ KJ} \quad (5)$$

The reaction of PbS for the formation of the S^{2-} ion and elemental Pb is therefore

$$Pb + S^{2-} \Leftrightarrow PbS + 2e \qquad \Delta G^o = +179.49\text{ KJ} \quad (6)$$

Addend (5) and (6)

$$[Pb(NH_3)_4]^{2+} + Pb + S^{2-} \Leftrightarrow PbS + Pb^{2+} + 4NH_3$$
$$\Delta G^o = +335.48\text{ KJ} \quad (7)$$

$$S + 2e + 2H^+ \Leftrightarrow H_2S \qquad \Delta G^o = -27.40\text{ KJ} \quad (8)$$

Addend (7) and (8), changing the sense of (8) and added with (7)

$$[Pb(NH_3)_4]^{2+} + H_2S + S^{2-} \Leftrightarrow PbS + 4NH_3 + S + 2H^+ + 2e$$
$$\Delta G^o = +362.88\text{ KJ} \quad (9)$$

$$HPbO^- + H_2O + 2e \Leftrightarrow Pb + OH^- \qquad \Delta G^o = +436.61\text{ KJ} \quad (10)$$

Addend (9) and (10)

$$HPbO^- + H_2O + [Pb(NH_3)_4]^{2+} + H_2S + S^{2-} \Leftrightarrow PbS + 4NH_3 + S + 2H^+ + Pb + OH^- + Pb^{2+}$$
$$\Delta G^o = +799.48\text{ KJ} \quad (11)$$

Since $\Delta G^0 > 0$, and as such, the reaction is not a spontaneous process. Reversing the direction of the reaction (6), ΔG^o changes its sign:

$PbS \Leftrightarrow 2e + Pb + S^{2-}$ ΔG^0= - 179.4 KJ (12)

For sulfur ion

$S^{2-} \Leftrightarrow S + 2e$ ΔG^0 = +86.272 KJ (13)

Adding (4), (5) and (6), the reaction for the PbS is obtained:

$Pb + 2S^{2-} + H^+ \Leftrightarrow PbS + HS^-$ ΔG^0= - 120.50 KJ (14)

$PbS + 2e + 2H^+ \Leftrightarrow Pb + H_2S$ ΔG^0= + 177.66 KJ (15)

$Ni^{2+} + 2e \Leftrightarrow Ni$ ΔG^0= +48.250KJ (16)

$Ni + 2OH^- \Leftrightarrow Ni(OH)_2 + 2e$ ΔG^0= -138.96 KJ (17)

$Ni(OH)_2 \Leftrightarrow Ni^{2+} + OH^-$ ΔG^0= 90.71 KJ (18)

Adding (14), and (18), the reaction for the PbS:Ni^{2+} entity is obtained:

$Pb + 2S^{2-} + Ni(OH)_2 \Leftrightarrow PbS + HS^- + Ni^{2+} + OH^-$

ΔG^0 = - 29.79 KJ (19)

$Cd^{2+} + 2e \Leftrightarrow Cd$ ΔG^0 = - 77.75 KJ (20)

$Cd(OH)_2 + 2e \Leftrightarrow Cd + 2OH^-$ ΔG^0 = - 156.13 KJ

Based on the Gibbs free energy values obtained from the thermodynamic equilibrium analysis, the Ni^{2+} and Cd^{2+} ionization state probably is present in the volume of PbS under our work conditions comparing the changes in ΔG^0, which thermodynamically enable to the growth of the PbS:Cd^{2+} and PbS:Ni^{2+}. Deposition includes different limiting physical and chemical processes which determine the kinetic behaviour of the doped PbS. (*i*) **Nucleation stage**. It is the initial stage requiring a high activation energy in which reactive centres (nuclei) are formed on the surface on the substrate. (*ii*) **Growth stage**. It is the second stage, which is characterized by an enhanced rate of PbS deposition. (*iii*) **Doped stage**. The high rate of deposition is associated with the addition level of doping, whit the accelerated growth of PbS doped nuclei formed on the substrate during the nucleation stage. (*iv*) **Termination stage.** During this stage, the rate of deposition gradually slows daw. This is probably due to a depletion of the reagents in deposition mixture.

The glass substrates were previously immersed in a $K_2Cr_2O_7$/HCl/H_2O solution for 24 h, after which they were rinsed in deionised water and dried in a clean hot–air flow. Preparation of polycrystalline doped PbS thin films on glass substrates was performed at a temperature of 20 ± 2°C undoped and doped with $V_{[Ni2+]}$ grown by chemical bath deposition (CBD) and pH = 11.0. The growth of PbS films with six different levels of doping $V_{[Ni2+]}$ were obtained by the addition in situ: 2, 4, 6, 8, 10, 12 mLs in the solutions for PbS growth $Pb(CH_3CO_3)_2$ (0.01 M), KOH (0.5 M), NH_4NO_3 (1.5 M), $SC(NH_2)_2$ (0.2 M). The solutions were mixed and the final

solution heated at 80 ± 2°C during 2 h, with the substrate remaining inside the solution. The optimal concentration of the doping solution [$V_{[Ni2+]}$] $Ni(NO_3)_2$ (0.023 M) was determined after several trials, until films had attained good adherence. This solution is routinely added to the reaction mixture during the growth of the PbS films. The samples were labelled as PbSNi0 for the undoped sample, PbSNi2-PbSNi12 for the doped samples. The total volume of the growing-solution consisted of the volume-solution (V_{PbS}) for the PbS growth plus the volume-solution $V_{[Ni2+]}$ containing the doping Ni^{2+} chemical agent: $V_{PbS} + V_{[Ni2+]} = V_{tot}$. The relative volume $V_{[Ni2+]}$ changed from 2 to 12. The films were growing obtained were silver-colored, polycrystalline-reflective, with a homogeneous consistency and good adhesion to the substrate. PbS thin films on substrates on glass substrates at 80 ± 2°C doped with Cd^{2+} grown by chemical bath deposition (CBD) was performed at a temperature of 80 ± 2°C undoped and doped with $V_{[Ni2+]}$ grown and pH = 11.0. We growth PbSCd films with five different levels of doping of Cd^{2+}: 2, 4, 6, 8, 10 ml. The solutions used for PbS growth: $(CH_3COO)_2Pb$ 0.01M, 0.5M KOH, 1.5M NH_4NO_3, $SC(NH_2)_2$ 0.2M and the doping solution ($V_{[Cd2+]}$) was $CdCl_2$ at optimal concentration 0.02 M. The growth of PbSCd films with five different levels of doping $V_{[Cd2+]}$ were obtained by the addition in situ: 2, 4, 6, 8, 10 mLs in the solutions for PbS growth. All the solutions used were prepared with deionised water of resistivity 18.2 MΩ. The films were growing using three sequential baths. The films were of silver-grey colour, homogeneous, polycrystalline reflective and with good adhesion to the substrate [18, 19].

3. Results and discussion

3.1. Scanning Electron Microscopy (SEM)

The semi-quantitative analysis of the films was carried out by using the EDAX technique for undoped and doped PbSCd and PbSNi thin films at different points to study the stoichiometry of the films. In Table 1 are displayed the atomic concentrations of Pb, Si and Cd obtained from Scanning Electron Spectroscopy (SEM).

	Atomic concentrations		
Sample	Pb	S	Cd
PbSCd0	56.35	43.05	0.0
PbSCd6	60.10	18.38	21.51
PbSCd10	56.29	33.49	10.22

Table 1. Atomic concentrations of Pb, S and Ni obtained from EDAX

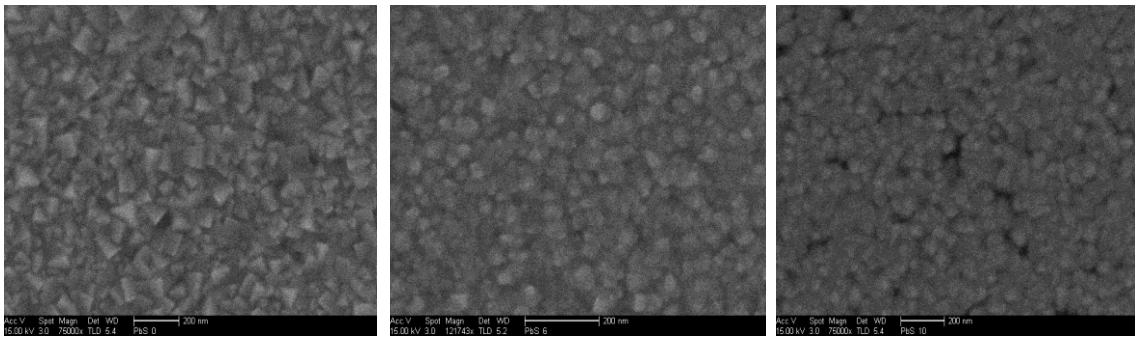

(a) (*b*) (*c*)

Figure 3.1. Micrographs of the films: (*a*) undoped PbSCd0, (*b*) doped with 6mLs PbSCd6 (*c*) doped with 10 mLs PbSCd10.

The morphological analysis of the PbSCd films was carried out in SEM micrographs is show in Figure 3.1. (*a*) Micrographs of the films undoped, (*b*) doped with 6mLs, (*c*) doped with 10 mLs. You can see the uniform surface morphology, which is compact and polycrystalline [19]. The SEM micrographs show that the particle grain size decreases with $V_{[Cd2+]}$ concentration. The granules are made of different sizes; we can conclude that the doping plays a vital role on the properties of the PbSCd thin films. The micrographs of the films with doping levels of 2, 4 and 8 mLs, are not shown. The these micrographs are appreciated for the films which undoped, and which have compactly highly reflective characteristics of the PbS obtained by means of the technique CBD [20], and those that doped have crystals in the form of spheres. A very adherent film with gray-black colour metallic aspect was obtained in case of a undoped and doping PbSCd films reveal a continuous compact polycrystalline films with similar morphology have been reported using a scale of 400 nm [21]

	Atomic concentrations		
Sample	Pb	S	Ni
PbS-Ni0	56.35	43.05	0.0
PbS-Ni6	70.10	18.38	11.51
PbS-Ni12	56.29	33.49	10.22

Table 2. Atomic concentrations of Pb, S and Ni obtained from EDAX.

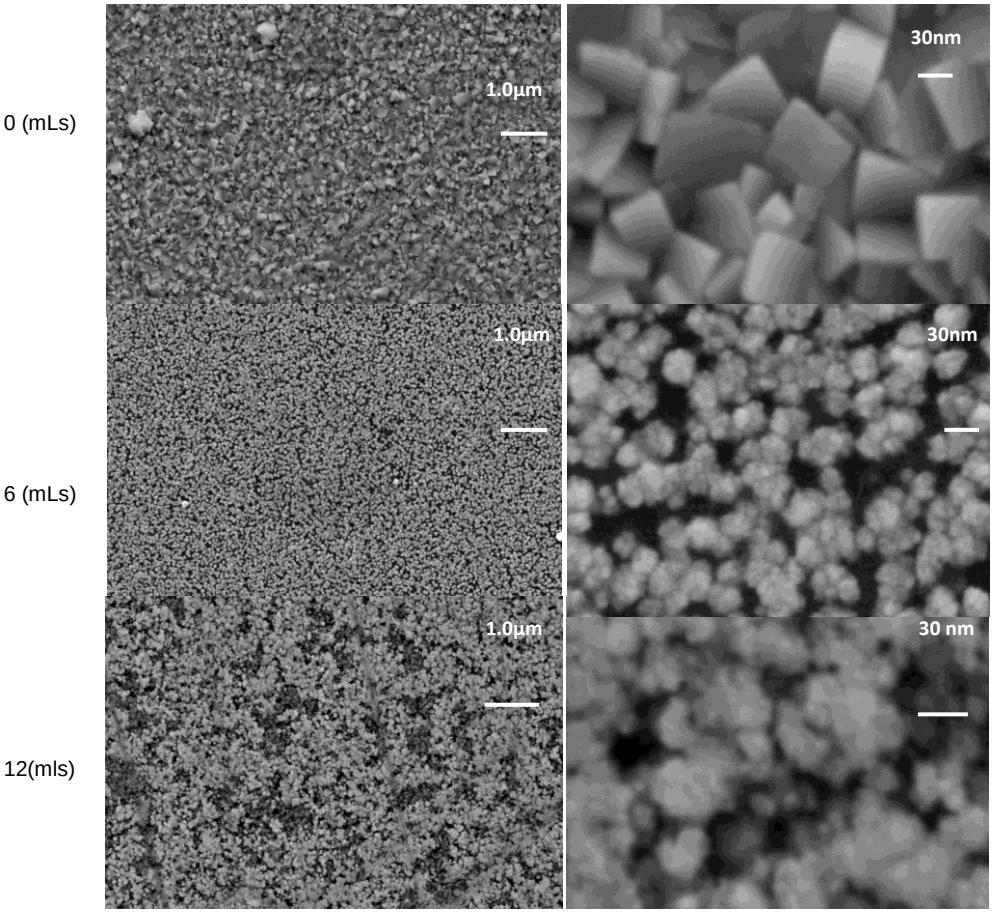

Figure 3.2. Micrographs obtained from SEM of the films with scales of 1.0 µm and 30 nm for undoped-PbSNi0, PbSNi6 and PbSNi12 films

In Table 2 are displayed the atomic concentrations of Pb, S and Ni obtained by SEM [22]. For the samples the increase in concentration of Ni in PbS films is easily noted. In this case, when Ni^{2+} ion enters as a substitute of the Pb^{2+} ion, it is observed that the sample was slightly deficient in S^{2-} ion. Therefore, for the higher $V_{[Ni2+]}$ values considered here, growth material can probably be estimated as doped semiconductor but actually the material can be regarded as similar to $Pb_{1-x}Ni_xS$ solid solution. It can also be considered how the concentration of Ni in PbS films increase, reaching a percent value of Ni = 11.51. In this case, when the Ni^{2+} ion enters as substitute of the Pb^{2+} ion, probably for the higher $V_{[Ni2+]}$ values considered here the growth material can also be estimated as a doped semiconductor being the material also as in the aforementioned conditions-similar to a solid solution of $Pb_{1-x}Ni_xS$. The micrographs of undoped-and doped-PbS films are showed in Figure 3.2. Scale bar at 1.0 µm, and 30 nm respectively were obtained by SEM.The undoped-PbS0Ni, doped-PbSNi6 (with 6mLs), doped-PbS12Ni (with 12mLs) films are showed. As can be seen from the uniform surface morphology, such aspect is compact and of polycrystalline nature. The SEM micrographs show that the particle grain size decreases with an increase in $V_{[Ni2+]}$ concentration. The granules appeared to be of different sizes. The micrographs of the films with doping levels of $V_{[Ni2+]}$ 2, 4, 8 and 10 mLs are not shown. In such micrographs for the undoped films, crystals as small spheres are observed. A very adherent film with metallic

gray-black colored aspect was obtained for undoped and doped films revealing continuous and compact polycrystalline films. Similar morphologies have been reported [21].

3.2. X-ray Diffraction (XRD)

Figure 3.2.1 shows sample diffractograms of X-ray for doped and undoped PnSCd films. These spectra of X-ray, show peaks located at the following angular positions: 2θ = (26.00, 30.07, 43.10, 51.00, 53.48). Diffraction along the [111] plane shows the highest intensity well-defined sharp peak, indicated high crystallinity of the material prepared. These belong to the wurzite phase according to reference patterns JCPDS 05-0592. The spectrum of films PbSCd04, shows two peaks located in the angular positions of 2θ = [27.25, 28.49], which belong to the PbO in monoclinic phase, according to the standards JCPDS 019-0697, and another peak in 2θ = [34.04], which corresponds to PbO in orthorhombic phase according to the standards JCPDS 052-0772. PbO was favored according to the following reaction

$$PbO_3^{2-} + H_2O + 2e \Leftrightarrow PbO + 2OH^-$$

By mean of CBD, E. Pentia *et. al*. [21] proposed the formation of PbO as a process of absorption according to the following reaction:

$$PbO_3^{2-} + OH^- \Leftrightarrow PbO + 3H_2O + 2e \qquad \Delta G^0 = +111.94\ \text{KJ}$$

A deeper research in the theme will be significant in future. However, in our work, we only generate this oxide in PbSCd4 and PbSCd8 samples. Other authors using the spray pyrolysis identified mix of phase control of the mole fraction *x* getting a solid solution of $(CdO)_{1-x}(PbO)_x$ [6, 22].

In set Figure 3.2.1 is exhibited the average grain size (GS) of PbS for the sample that was undoped and the doped one corresponding to the [111] plane against the volume of the doping ($V_{[Cd2+]}$). For the PbSCd8 film can be seen at a relative minimum of 28 nm. In this plot, it is possible to see that the GS decreases for the sample PbSCd2 and remains without change for 4, 6, 10 mLs of 34 nm.

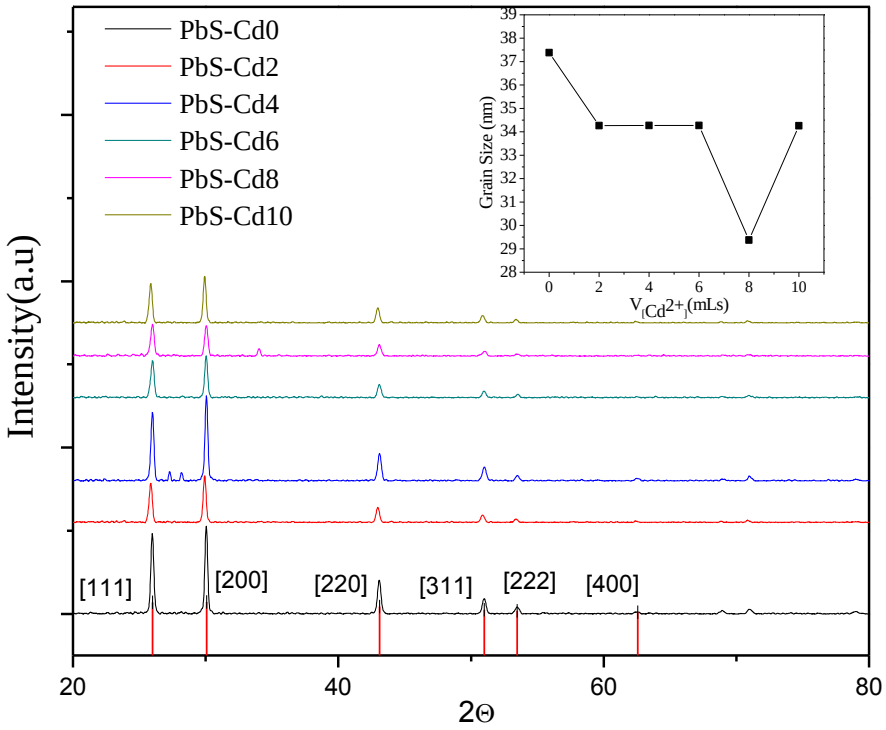

Figure 3.2.1. XRD patterns of the undoped and PbS doped Cd^{2+} films. From V = 0 to V 10 mLs the patterns are placed consecutively**.**

The effect of the decrease of the GS by the effect of the doping has been reported in films of CdS doped with Cu^{2+} by CBD [22]. A possible explanation to this experimental fact can be given as it follows: The ionic radii data are Pb^{+2} = 1.21 Å, $S^{2=}$ = 1.84 Å and Cd^{2+} = 0.95 Å, for relative low concentration Cd^{2+} ions can be majority situated in (*i*) Pb^{2+} vacancies sites which otherwise would be empty (*ii*) in Pb^{2+} sites provoking the appearing in Pb interstitial, and (*iii*) in interstitial positions. At this level of Cd^{2+} the PbS can be considered a doped material [18, 19, 22]. That tendency to amorphize the material makes the localized monocrystalline zones (grains) become smaller and smaller as Cd^{2+} increases, give nanocrystals. The dimensions of the crystallites depend on the experimental parameters namely pH, concentrations of reactants, temperature, substrate and doping. In this work, adding to the starting solution a small quantity of doping changes in a crystallites order and/or alteration of their size can be observed. A decrease in the degree of order of crystallites, this is expected to lead to enhanced growth of stable nuclei in the initial stages of growth followed by impaired grain growth, hence, resulting in smaller grains in the cadmium.

Figure 3.2.2 shows diffractogram of X-ray (XRD) for doped and undoped PbSNi films. Such x-ray spectra display peaks located at the following angular positions: 2θ = (26.00, 30.07, 43.10, 51.00, 53.48). They are related with the reflection peaks of [111], [200], [220], [311], [222] respectively, and all these diffraction peaks can be perfectly indexed to diffractogram of the undoped and doped PbS samples displaying the zinc blende (ZB) crystalline phase according to reference patterns JCPDS 05-0592. The XRD spectra for PbSNi2 films indicate that [111] is the orientation of PbS Ni grains; the PbSNi2 diffraction layer along the [111] plane reveals the highest intensity of a well-defined sharp peak, indicating the high crystallinity of the obtained material.

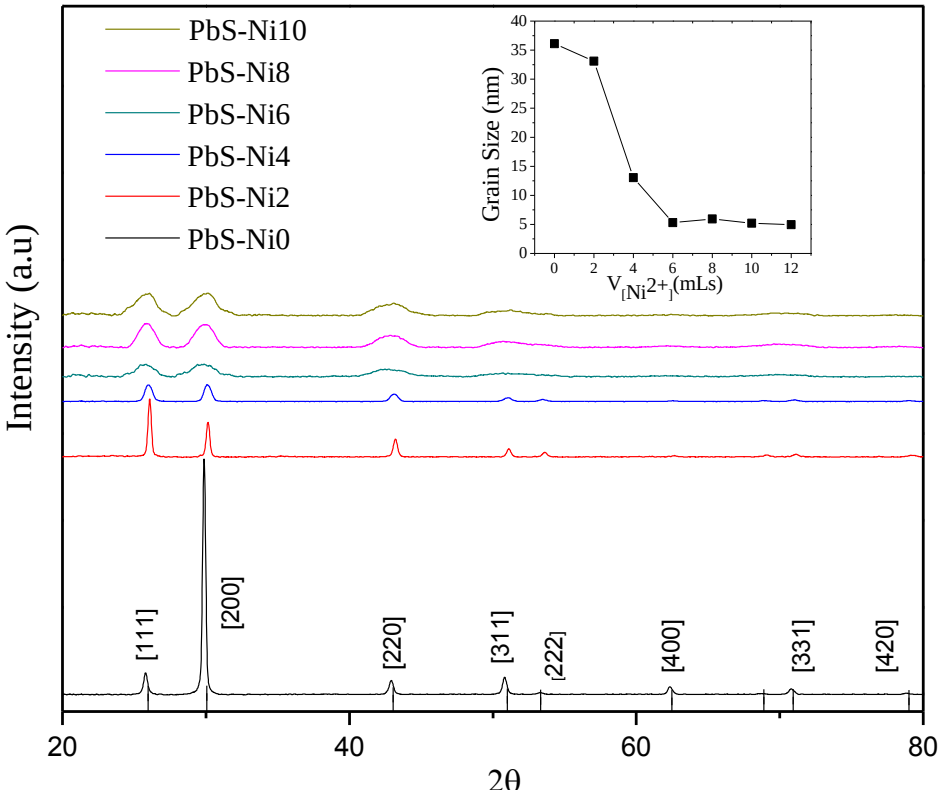

Figure 3.2.2. XRD diffractograms for doped Ni^{2+} and undoped-PbS films. The patterns are placed consecutively. The inset illustrates the [111] reflections of the cubic phase as function of $V_{[Ni2+]}$,

A maximum value in the intensity peak is reached for the prepared sample, indicating either the existence of a larger number of [111] planes or that the [111] planes have a lower number defects. The relative intensities for PbSNi2 and PbSNi4 layers for [111], [200], [220] are nearly equal and all the representative diffraction lines of PbS can be observed. In the PbSNi2 film, the [111] reflection has the highest intensity. This phenomenon may be attributed to the doping effect. The low intensity peaks observed in the XRD patterns of the doped PbSNi6 to PbSNi12 samples indicates that the films are coarsely fine crystallites or nanocrystalline. The broad hump in the displayed pattern is due to an amorphous glass substrate and also possibly due to some amorphous phase present in the PbSNi crystallite size of films. These effect are associated whit the nanocrystals doped-PbSNi with $V_{[Ni2+]}$ in the regime were the cluster mechanism is dominating (on the contrary to films grown via ion-ion mechanism, were the crystal size was larger), and consist of PbSNi nanocrystals embedded in an apparent matrix of PbS. In set Figure 3.2.2 show that average grain size (GS) with of the mean peak of XRD patterns vs. $V_{[Ni2+]}$. The inset exhibits the E_g vs GS plot. A decrease in the degree of order of crystallites is expected to lead to enhanced growth of stable nuclei at the initial stages of growth, followed by impaired grain growth, and hence

resulting in smaller grains in the nickel. A possible explanation to this experimental fact can be given as follows: The ionic radii data are Pb^{+2} = 1.21 Å, S^{2-} = 1.84 Å and NI^{2+} = 0.69 Å, therefore for a relative low concentration of Ni^{2+} ions a majority can be located in (*i*) Pb^{2+} vacancies sites, which otherwise would be empty (*ii*) in Pb^{2+} sites causing the appearance of Pb interstitial, and (*iii*) in interstitial positions. At this level of $V_{[Ni2+]}$, the PbSNi can be considered a doped material [18]. The incorporation of Ni^{2+} solubility has been proven to be more effective in Pb chalcogenide than Zn-chalcogenide, a result explained in terms of the cation size.

3.3. Optical absorption (OA)

The energy gap (E_g) of the samples was determined from optical transmission. From the transmission data, the absorption coefficient was calculated in the region of strong absorption using the formula according to Swanepoel [24]

$$\alpha = \frac{1}{d} ln \frac{A}{T}$$

Where *T* is the transmission

$$A = \frac{16n^2}{(n+1)^2(n+s)^2}$$

Where *T* is the transmission, the refractive index of glass an the refractive index of the layer *n* were assumed to be constant in the region of strong absorption. The refractive index *n* and the thickness *d* of the layer were estimated from the reflection spectra. Assuming parabolic band structure, the absorption coefficient α is proportional to

$$\left(E - E_g\right)^{\frac{1}{2}} = \alpha h\gamma$$

And an extrapolation to $\alpha^2 = 0$ yields a good approximation of the energy gap (E_g) [25]. The optical property of materials information is obtained using the technique. With this technique it is possible to plot the percentage (%) of the transmittance vs. the wavelength (λ), and by using the Planck equation $E = \frac{hc}{\lambda}$, the energy of the incident photon for each value of the wavelength of light is expressed in terms of the energy of the photon incident in this way is the spectra of (%) of T vs. the energy of the incident photon and where *T* + *R* = 100, where *T* is the transmittance and *R* the reflectivity of the film.

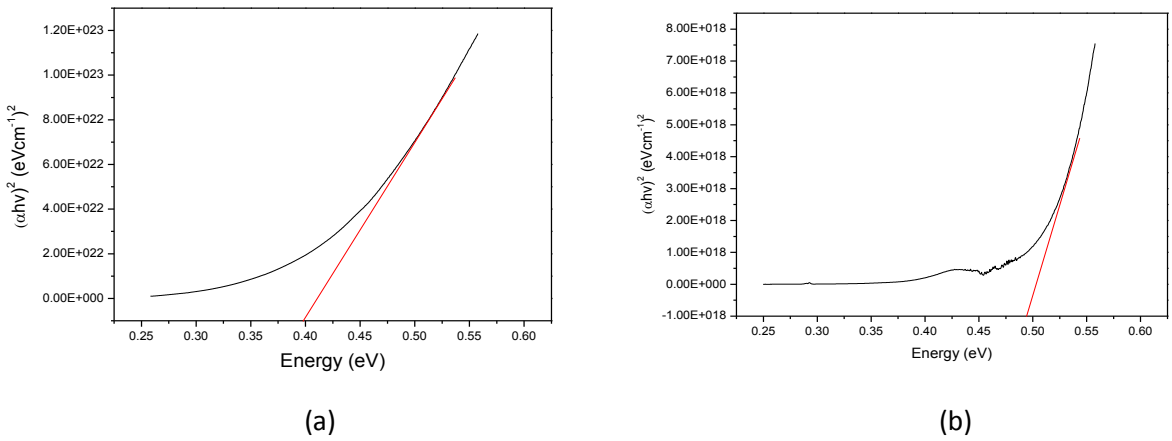

Figure 3.3.1. Optical Absorption spectra for the sample (*a*) PbSCd0 y (*b*) PbSCd10.

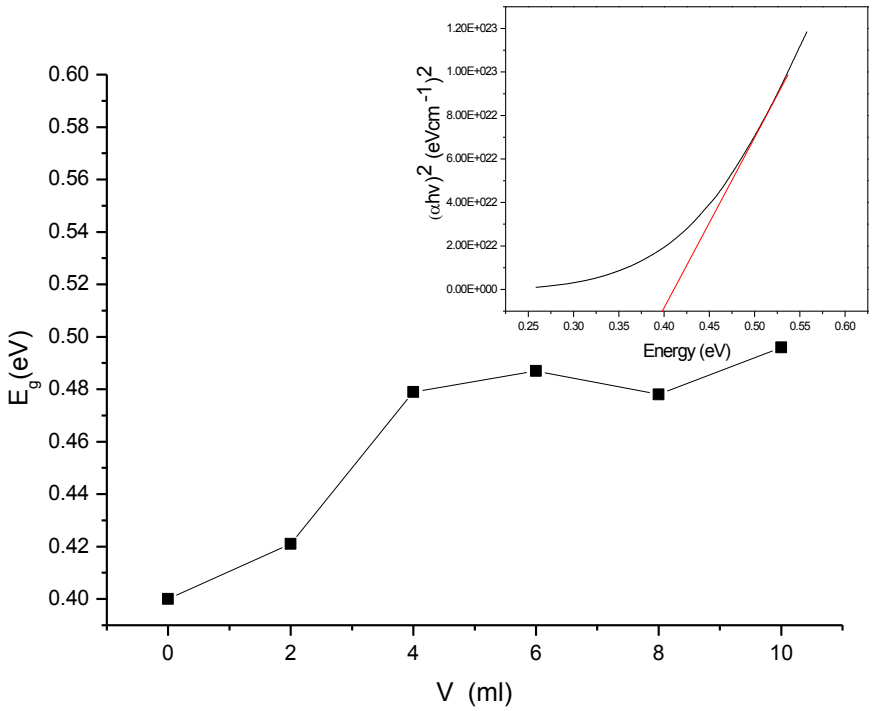

Figure 3.3.2.. Band gap energy (E_g) for fhe fundamental absorption, as function of doping volume in 0.25-0.60 eV range, in doped and undoped PbS, inset illustrates the method to calculate from optical absorption measurements.

Figure 3.3.1 shows the spectra of the optical absorption for the samples (*a*) PbSCd0. (*b*) PbSCd10. The fundamental absorption which corresponds to electron excitation from the valence band to conduction band can be used to determine the nature and value of optical

band gap. For the simple PbSCd0, through the intersection of the straight line with the axis of the photon energy is obtained $E_g = 0.40$ eV and in a similar way to the sample PbSCd10 $E_g = 0.51$ eV.

The Figure 3.3.2 shows E_g vs. the Cd^{2+}doping and the upper right part of the same plot shows the spectrum of absorption for the sample undoping. In this plot, it can be observed that the sample of PbSCd2 has a relative minimum of E_g = 0.34 eV. The shift experimentally observed E_g values indicated alloying between nanocrystalline PbS and CdS phases. The figure 3.3.3 illustrates the forbidden band gap Ni^{2+} layers 2.2-3.0 eV range, the large experimentally observed E_g in the nanopartcle films to theorically estimated (using Vegar'ds law) E_g for bulk shows the extent of quantum size effect in nanoparticle films. It is seen that size effect on the optical band gap is stronger nanoparticle films than in PbS nanoparticles of 24 nm, which is 3.4 times the E_g for bulk PbS [2].

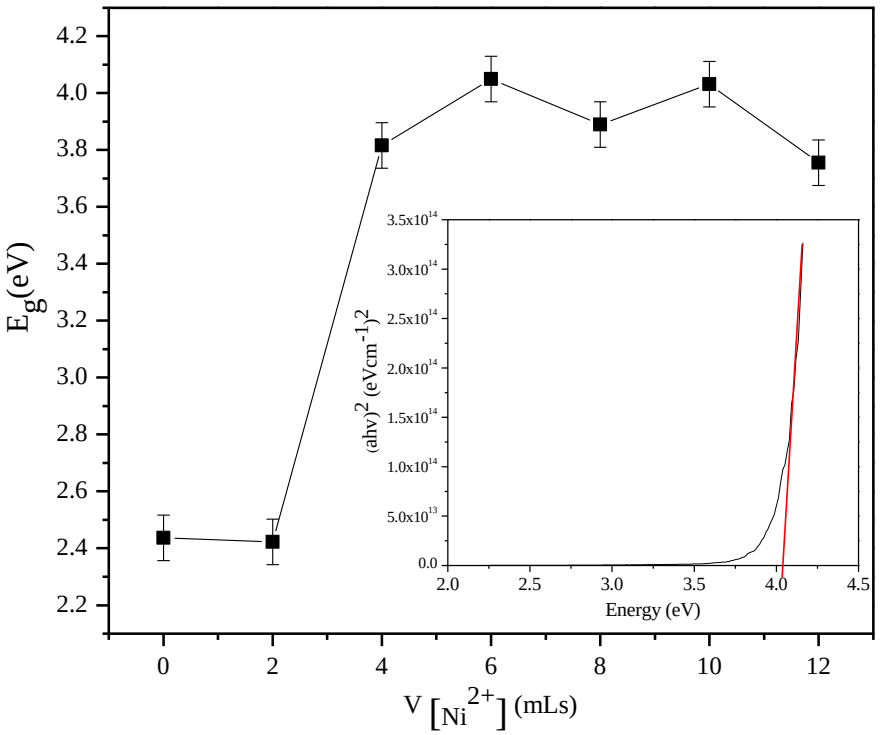

Figure 3.3.3. Band gap energy as function of Ni^{2+} doping volume in 2.2-4.0 eV range, in doped and undoped PbS, the inset illustrates the method to calculate from optical absorption measurements**.**

Figure 3.3.3 shows a graph of E_g vs $V_{[Ni2+]}$ and in the inferior right part the plot shows the absorption spectrum for the sample PbSNi12. In this plot, it can be observed a E_g = 2.4 eV value for the PbSNi0 sample.The confinement effect appears as a shift in edge of the absorption spectra and the absorption to lower wavelengths, possibly due to the decrease in GS, the decrease in number of defects and the change in color. It is clearly seen from the optical spectrum an absorption edge shift toward a lower wavelength in doped films. The

experimentally observed E_g values for the shift indicated an alloying between nanocrystalline PbS. Such increase has been observed by other authors [2, 9]. The E_g for doped samples in the 2.4-3.8 eV range the large experimentally observed E_g in the nanoparticle films theoretically estimated (using Vega*r*'ds law) E_g for bulk shows the extent of quantum size effect in the nanoparticle films. The fundamental optical transition of doped films (E_g = 0.41 eV) is not observed in these films, presumably because of complete mixing of PbS with Ni^{2+} affording an unique ternary intermetallic compound of the $Pb_xNi_{1-x}S$ type [19]. It is observed that the size effect on the E_g is stronger in nanoparticle films than in PbS nanoparticle of 24-10 nm (average crystallite size) and show an E_g: 2.22-2.65 eV [2]. The observed increase in the quantum size effect could possibly be attributed to a decrease in the effective mass [23]. The increased in E_g when increasing the concentration of $V_{[Ni2+]}$ in the films is reflected by the presence of an excitonic structure material. Excitonic structures are readily observed in large E_g semiconductors with binding energy such as CdSe [24]. The E_g optical doped films varied from 2.4-3.8 eV, with doping increase of $V_{[Ni2+]}$. A similar shift observed in the position of the excitonic peak towards higher energies in CdSe crystallites has been explained due to a decrease in crystallite size [25]. The redshift of the band gap is associated with the decline of the SG. It is clear that the E_g increase when $V_{[cd2+]}$ and $V_{[Ni2+]}$ increases. As mentioned earlier, we observed a systematic decrease in the crystallite size with increasing concentration. Since the estimated mean crystallite size in this case being approximately half the value of the exciton Bohr radius in PbS, we observe a strong confinement in doped PbSNi films and weak confinement in doped PbSCd. Using already published data, a nanocrystalline size of 4-5 nm corresponding to E_g = 1-1.25 eV, 3.8 nm for E_g = 1.4 eV, 2.7 nm for E_g = 2.0 eV and 2 nm for E_g = 2.7-3.8 eV respectively are obtained [22]. Figure 6 shows the average grain size (GS) vs. $V_{[Ni2+]}$ for the undoped- and doped PbS samples corresponding to the [111] plane. Can be observed that GS reduces in the interval 4mLs ≤ $V_{[Ni2+]}$ ≤12mLs. It can be seen for the PbSNi0, GS ~32 nm, and that the GS decreases for doped samples.

Conclusions

Doped-PbS films with Cd^{2+} and Ni^{2+} ions affording nanocrystalline films by CBD. X-ray spectra show 2θ = (26.00, 30.07, 43.10, 51.00, 53. 48), which belong to the ZB phase in two layers. The grain size lies in the interval of ~32-5 nm for PbSNi. Redshift of band gap is associated with the decrease of the average TG. The E_g of films increased from 2.4-3.8 eV when doping $V_{[Ni2+]}$ is increased. GS reduces in the interval 2mLs ≤ $V_{[Ni2+]}$ ≤12mLs and E_g increase as function of the GS is displayed. When GS ≅ 5 nm, The spectra of PbSCd04 films show two peaks which are located in the angular position at 2θ = (27.25, 28.49), which belong to the PbO in a monoclinic phase and another peak in 2θ = (34.04), which corresponds to PbO in an orthorhombic phase. E_g reaches a maximum value; for larger GS, E_g decrease. Optical Absorption Spectra is quantified for the film PbSCd10 film which is undoped, and it happens to be E_g = 0.51 eV. The optical band gap PbSNi films varied from 2.1-4.0 eV, wit increase doping Cd^{2+}. In this research two effects occur on E_g changes: We observe a strong confinement in doped PbSNi films and weak confinement in doped PbSCd.

Acknowledgements

The authors thank N. Melgoza Palma, Secretaria Académica de la Fac. de Ciencias Químicas of the Benemérita Universidad Autónoma de Puebla, for the support given to the publication of this research.

References

[1] Alex Gaiduc, Peter I. Gaiduk, Arne Nylandsted Larsen, Thin Solid Films **516** (2008) 3791-3797.
[2] K. Rakesh, H. A. Joshi, H. K. Sehgal, Nanotechnology **14** (2003) 809-812.
[3] Y. F. Nicoles, Dupuy M. J. Electrochem. Soc. **137** (1990) 386-392.
[4] Ray S. C., Karanjai M. K., D. Dashupta Thin Solid Films, **332** (1998) 117-122.
[5] L. Deshmukh, K. M. Garandakar, D. S. Sutrave, Materials Chemistry and Physicshttp://www.sciencedirect.com/science/article/pii/S0040609097009322 - cor* **55** (1998) 30-35.
[6] O. Portillo Moreno, H. Lima Lima, V. Ramírez Falcón, J. Martínez Juárez, G. Juárez Díaz, R. Lozada Morales, R. Rebollo Plata, R. Palomino Merino, A. B. Soto Guzmán, O. Zelaya Ángel, J. Electrochem. Soc., **153** (2006) 926-930.
[7] V. M. García, M. T. S. Nair, P.K, Nair Sol. Energy. Mater. Sol. C. **23** (1991) 47-59.
[8] J. B. Biswal, N. V. Sawant, S. S. Garje**,** Thin Solid Films **518** (2010) 3164-3168
[9] K. Rakesh, A. K. Joshi, H. K. Shegal, Appl. Surf. Sci. **221** (2004) 43-47.
[10] S. Thangavel, S. Ganesan, S. Chandramohan, P. Sudhgar, Yong Soo Kang, Chang-Hee Hong, Journal of Alloys and Compounds **495** (2010) 234-237.
[11] M. Wanili, J. M Luther, H. Zheng, Y. Wu, P. Alivisatos, Nanoletters, **9** (2009) 1699-1703.
[12] Sixin Wu, Hongxia Zeng, and Soltan A. Schell, Langmuir, **21** (2005) 686-700.
[13] J. Ju, D. Cui, T. Zhu, G. Paradee, Z. Liang, Q. Wang, S. Y. Xu, A. Y. Wang Nanotechnology, **17** (2006) 1699-1703.
[14] A. Dittmer, P. Alivisatos, Science **295** (2002) 5428-5434.
[15] Pietryga J.M, Schaller R.D, Werder D., Stewart M. H, Klimov V. I., Hollingsworth J. A. J. Am. Chem. Soc. **126** (2004) 11752-11756.
[16] J. Bethune, N. A. S Loud. in *Standard Aqueous Potential an Temperature Coefficients at 25 °C*, C. C. (1969) Hampel, Skokie, II.
[17] O. Portillo Moreno, G. Abarca Ávila, J. R. Cerna, J. Hernandez Tecorralco, M. Chavez Portillo, R. Lozada Morales, O. Zelaya Angel, Journal of Materials and Engineering **A 1** (2011) 692-704.
[18] O. Portillo Moreno, L.A. Chaltel Lima, M. Chávez Portillo, S. Rosas Castilla, M. Zamora Tototzintle, G. Abarca Ávila, R. Gutiérrez Pérez, IRSN Nanotechnology, **1** (2012) 1-12.
[19] O. Portillo Moreno, M. Chávez Portillo, M. Moreno Flores, J. Martínez Juárez, G. Abarca Ávila, R. Lozada Morales, O. Zelaya Ángel, Journal of Materials and Engineering **A 1** (2011) 759-767.
[20] A. Popa, M. Lisca, V. Stancu, M. Buda, E. Pentia, T. Botilae, Journal of Electronics and advanced materials **18** (2006) 43-45.

[21] E. Pentia, L. Pintillie, T. Botila, I. Pentille, A. Chaparro, C. Maffiotte, Thin Films **434** (2003) 162-170]
[22] M. Chávez Portillo, J. Martínez Juárez, G. Abarca Ávila, M. Zamora Tototzintle, M. Martínez Barragán, J. R. Cerna, M. Lazcano Hernández, S. Rosas Castilla, B. Crespo Sánchez, A. Celeste Palacios López and O. Portillo Moreno, Journal of Materials Science and Engineering **A 1** (2012) 759-767.
[23] B. Thangaraju, P. Kaliannan, Semicond. Sci. Technol. **15** (2000) 542-544.
[24] R. Swanepoel, J. Phys. E **16** (1983) 1214-1216.
[25] I. Balberg, E. Savir, Y Dover, O. Portillo Moreno, R. Lozada Morales, O. Zelaya Ángel, Phys. Rev. **B 75** (2007) 153301-4.